Results in Engineering 22 (2024) 102279

Contents lists available at ScienceDirect

Results in Engineering

journal homepage: www.sciencedirect.com/journal/results-in-engineering

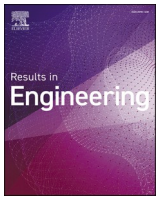

A dual ultra-wideband rectenna with a compact conical antenna for RF energy harvesting from S and C bands

Shailendra Singh Ojha [a], Jai Kumar Sharma [b], Bhupendra Dhakad [c], Sateesh Kumar [b], Neeraj Sharma [a], Anuj Kumar Pandey [d,*], S.M. Mozammil Hasnain [e], Sandeep Kumar [f,***], Rahul Kumar [g,**]

[a] Department of ECE Ajay Kumar Garg Engineering College Ghaziabad, (U.P.), 201015, India
[b] Department of Mechanical Engineering, ITM University, Gwalior, India
[c] Department of ECE, ITM University Gwalior, (M.P.), 474005, India
[d] Department of Computer Science and Engineering, Birla Institute of Technology, Mesra, Ranchi, 835215, India
[e] Faculty of Engineering and Applied Science, Usha Martin University, Ranchi, 835103, India
[f] Centre of Research Impact and Outcome, Chitkara University, Rajpura, 140417, Punjab, India
[g] Chitkara Centre for Research and Development, Chitkara University, Himachal Pradesh, 174103, India

ARTICLE INFO

Keywords:
Conical antenna
Ultra-wideband
RF energy harvesting (RFEH)
Rectenna
Conversion efficiency

ABSTRACT

The current research introduces a novel dual ultra-wideband rectenna that has been specifically devised for the S and C bands. The rectenna configuration being presented demonstrates the potential to efficiently capture energy from 1.5 GHz to 4.65 GHz, and 5.55 GHz–7.85 GHz. It is noteworthy to mention that the bandwidths (BW) corresponding to these frequency ranges are 3.15 GHz and 2.3 GHz, correspondingly. The envisioned rectenna is designed to cater to a selection of five distinct commercial bands. The frequencies under consideration include 1.8 GHz, UTMS 2.1 GHz, 5G 3.5 GHz, 4.5 GHz, and 5.8 GHz, which fall within the mid band range for 5G technology. Notably, the extended S-band and C band are also included within this range, catering specifically to 5G applications. For the purpose of rectification, a solitary HSMS 2850 Schottky diode has been selected. The maximum recorded Conversion Efficiency (CE) achieved at 1.8 GHz, 2.1 GHz, 3.5 GHz, 4.5 GHz, and 5.8 GHz corresponds to CE values of 67 %, 65 %, 77 %, 71 %, and 71 %, respectively. These CE measurements were obtained under varying input power levels (IPL) of −6 dBm, 4 dBm, 4 dBm, 2 dBm, and 9 dBm, respectively. The rectenna under consideration is designed to operate across five distinct frequency bands. Notably, the CE exceeds 65 % across all of these frequency bands. Consequently, the rectenna exhibits a higher output power. As a result, this modification makes it appropriate for supplying energy to low-power electronic equipment.

1. Introduction

The subject of RF Energy Harvesting (RFEH) has attracted considerable attention because of recent breakthroughs in the realm of technology. The proliferation of sensors across various domains can be attributed to the pervasive nature of the IoT. The current advancements in the field of IoT and contemporary sensor technologies have demonstrated remarkable potential. One significant drawback that persists is the reliance on batteries as a power source. This reliance imposes several constraints, including limitations on the range and duration of IoT devices, their environmental impact, and the challenges associated with replacing the batteries. This proposition serves as a catalyst for the conceptualization and development of an alternative methodology for the provisioning of power to sensory devices [1]. Energy harvesting from proximal sources and the transmission of power through wireless means, commonly referred to as wireless power transfer (WPT), represent two feasible approaches [2,3]. Energy harvesting refers to the systematic extraction of energy from various sources, including but not limited to wind, solar radiation, thermal gradients, water flow, and radio frequency signals generated by wireless communication systems [4–7].

* Corresponding author.
** Corresponding author.
*** Corresponding author.
E-mail addresses: anujpandey59@gmail.com (A.K. Pandey), sandeep.uietmdu@gmail.com (S. Kumar), rahulkumarmech84@gmail.com (R. Kumar).

https://doi.org/10.1016/j.rineng.2024.102279
Received 3 December 2023; Received in revised form 3 May 2024; Accepted 15 May 2024
Available online 18 May 2024

RFEH emerges as a viable and sustainable resolution for powering wearables, wireless sensor networks (WSNs), remote-deployed self--sustainable sensors (S3), portable Internet of Things (IoT) devices, and self-sufficient sensors [8]. Moreover, the widespread deployment of autonomous sensors across diverse sectors, including but not limited to agriculture, mining, healthcare, and urban infrastructure, has generated considerable scholarly attention towards the field of energy harvesting [9–12].

The primary advantage of RF harvesting lies in its capacity to effectively transform electromagnetic energy into electrical power, regardless of the time of day, location (whether indoors or outdoors), or environmental conditions. Moreover, the subterranean and intramural permeability of RF signals facilitates the acquisition of electromagnetic (EM) energy in locations where alternative energy reservoirs, such as solar and wind power, remain unattainable.

Considerable research efforts have been dedicated to the exploration of this particular domain, with a primary focus on the investigation of single band rectennas operating within the GSM [2,3], ISM [13], 5G band [14], and 5G mid band [15] frequency ranges. Nevertheless, the functionality of these harvesters will experience significant disruptions in the event of a shift in the ambient frequency. Moreover, due to the limited power availability associated with ambient radio frequency (RF) energy scavenging, the utilisation of energy harvester systems equipped with configurable impedance matching networks is not commonly deemed suitable [16].

The variability of ambient radio frequency (RF) power levels is contingent upon several factors, including the proximity to the broadcast cause, the characteristics of the communication medium, and the positioning of the antenna. Consequently, these aforementioned variables can give rise to unforeseen fluctuations in RF power levels within the surrounding environment. The crucial considerations pertaining to ambient energy scavenging encompass the effectiveness and sensitivity of an energy harvester (EH) [17]. If the system exhibits the capability to work across a broad spectrum of IPL and across multiple frequency bands, it possesses the potential to facilitate the concurrent transmission of signals across multiple bands and tones into an Energy Harvester (EH). This capability can be leveraged by employing the RF combining technique, thereby enabling the activation of the rectification device at lower input power levels that are typically present in the surrounding environment. Consequently, improves output DC power [18,19].

Huang et al. [20] proposed a rectenna design to optimise power utilisation, there is a growing focus on the development and implementation of multiband and wideband antennas. A microstrip line (MSL) is utilised to provide a small dual-band square slot loop operating at 2.4 and 5.8 GHz. An impedance matching network (IMN) is introduced in the intermediate region connecting the rectifier and the slot loop radiator to achieve a concurrent conjugate match at the two resonant frequencies owing to the distinct impedance characteristics exhibited at each resonance. A prototype of the proposed miniature slot loop rectenna designed for utilisation within the 2.4 and 5.8 GHz has been fabricated and subjected to experimental evaluation in order to validate its performance. Conversion efficiencies of 49 % and 66 % can be achieved.

Anh et al. [21] proposed a rectenna that can work at two frequencies ircuit under consideration operates within the frequency bands of 925 MHz and 2450 MHz, with the objective of harnessing RF power emanating from cellular and ISM communication systems [21]. By integrating two resonance structures, it is possible to achieve a reduction in the dimension of the rectifier section while simultaneously preserving an efficiency of up to 60 % across all frequency bands. Additionally, the rectifier component's antenna exhibits a reflection coefficient of −10 dB within 925 MHz and 2450 MHz. Moreover, it is noteworthy to mention that the antenna attains a comprehensive efficiency of 47 % at 925 MHz, while exhibiting an efficiency exceeding 80 % at 2450 MHz.

To enhance the efficiency of rectenna Dinh et al. [22] introduces a novel approach to enhance the efficiency and selectivity of triplexers utilised in triple-band energy harvesting. The proposed methodology focuses on the development of a triple band rectenna, which not only serves as a filter but also as a matching circuit for the aforementioned energy harvesting process. The efficacy of the triplexer in achieving favourable selectivity has been demonstrated, the proposed configuration contains of difficult-order open stubs, each having a length of (2n+1)/4., where n is an integer greater than or equal to 1. The triplexer proposed in this study demonstrates notable efficiencies of 92 % at 2.1 GHz. By incorporating the triplexer within the rectenna structure, it has been observed that the overall efficiency, when exposed to an IPL of 5 dBm, reaches a value of 60 %.

Rectenna that can target three band is presented by Hamza et al. [23] the proposed rectifier demonstrates the capability to efficiently capture energy from the 900/1800/2450 bands, particularly when operating within low to moderate ambient power densities. The proposed configuration consists of a trichotomous arrangement of parallel branches, collectively constituting a high-efficiency triple-band rectifier. The observed radio frequency (RF) to direct current (DC) conversion efficiencies are recorded as 33.7 %, 21.8 %, and 20 % at 0.9, 1.8, and 2.45 GHz (GHz), correspondingly. These measurements were obtained under the condition of an ideal load of 3.8 kΩ (kΩ) and an IPL of −10 dB mW. When subjected to IPLs of less than 0 dBm, the efficiency demonstrates a consistent performance exceeding 46.5 % across all relevant frequency bands.

Another triple band rectenna with good bandwidth is designed by Aboualalaa et al. [24] suggested antenna exhibits coverage over the frequency ranges of 1.86–2.65 GHz, 2.84–3.64 GHz, and 5.34–6 GHz. These frequency bands align with the impedance bandwidths of 35 %, 24.7 %, and 11.64 %, respectively, as determined through measurement analysis. When exposed to an IPL of 2 dBm, the CE of 69.7 % is achieved. The proposed rectenna exhibits a power conversion efficiency (PCE) exceeding 50 % within the range of IPL spanning from 6.5 to 4.7 dBm. Multiband rectenna proposed by Zhen et al. [25] demonstrates the capability to capture radio frequency (RF) power from multiple commercial bands. Specifically, the rectenna is designed to harness RF power from the following frequency bands: GSM, LTE, WLAN, 2.65 GHz for 5G, and 3.5 GHz for 5G, however, it provides low conversion efficiency. The CE exhibits notable performance at various frequencies. Specifically, at 1.8 GHz, the PCE achieves a commendable 23.1 %.

A seven-band omnidirectional rectenna for the purpose of RF energy harvesting was designed by Wang et al. [26], the proposed antenna demonstrates compatibility with a range of contemporary and advantageous frequency bands, namely GSM1800 (1.8 GHz), LTE (2.1 GHz), WLAN/Wi-Fi (2.4 and 5.8 GHz), as well as 5G bands (2.6, 3.5, and 4.9 GHz) but it provides low conversion efficiency. The present study introduces a groundbreaking seven-band rectifier, comprising a configuration of three parallel, meticulously optimised single shunt diode rectifiers, with the primary objective of generating a multiband antenna. At an IPL of −10 dBm, it is feasible to achieve CE up to 44.4 % at a frequency of 1.84 GHz. In the context of microwave power transmission and energy harvesting, a distinctive approach is employed wherein an ultra-wideband (UWB) rectenna incorporates a wideband complementary matching stub, resulting in a fractional bandwidth exceeding 100 % by Ping [27]. The proposed matching stub has the capability to exhibit the presence of "open" and "short" circuits in relation to frequency. The device employs an expansive frequency spectrum spanning from 0.9 to 3 GHz. At an IPL of 3 dBm, the CE grasps its maximum value of 73.4 %.

Potti [28] analysed a rectenna that is composed of a wideband rectifying circuit and a transparent Vivaldi antenna, enabling its operation from 3.1 GHz to 8 GHz. When subjected to an IPL of 10 dBm, the rectenna exhibits a maximum power CE of 69 %. The proposed antenna possesses the capability to be seamlessly integrated onto glass windows and automobile windscreens without impeding the user's typical visual field. An ultra-wideband (UWB) rectifier, which incorporates a high impedance inductor and a discone-based antenna, with the aim of enabling wireless power transfer. The discone antenna is renowned for

its exceptional capacity to cover a wide range of frequencies, while the rectenna's ability to operate in an ultra-wideband manner is facilitated by the utilisation of a high impedance inductor in the rectifier circuitry, thereby obviating the necessity for a matching network [29]. At 2.45 GHz and with an IPL of 5 dBm, the UWB rectenna demonstrates an efficiency of 16 %. Furthermore, it exhibits a coverage from 0.65 GHz to 5 GHz.

The utilisation of the CST MW Studio 2018 software is employed in the context of designing and simulating the envisaged dual wideband antenna. The utilisation of the ADS 2020 software is integral to the simulation, design, and optimisation of rectifiers. The fabrication procedure entails the utilisation of an FR-4 lossy substrate, characterised by a dielectric width of 1.6 mm and a dielectric constant of 4.4. Meanwhile, a conical pyramid structure is designed on a paper substrate, with an upper layer composed of copper.

The literature survey reveals a lack of emphasis on the development of multiband antennas with significant bandwidth and high gain, as well as efficient rectifiers capable of operating across many frequency bands.

The proposed work exhibits a distinct level of novelty in the subsequent fashion.

- First and foremost, in order to surpass the power capabilities of a single-band antenna, a decision has been made to employ a novel compact conical antenna for the purpose of receiving RF signals. This choice is primarily motivated by the antenna's inherent broadband characteristics.
- The proposed rectenna demonstrates operational efficiency from 1.5 GHz to 4.65 GHz, encompassing a bandwidth of 3.15 GHz. Additionally, it exhibits functionality from 5.55 GHz to 7.85 GHz, with a bandwidth of 2.3 GHz. This rectenna is specifically designed to cater to five distinct commercial bands, namely GSM 1.8 GHz, UTMS 2.1 GHz, 5G 3.5 GHz, 4.5 GHz, and 5.8 GHz 5G mid band (extended S-band and C band for 5G applications), concurrently.
- The utilisation of a three-line IMN and DC merging scheme is employed in order to augment the CE.
- In the context of a fabricated rectifier, the substitution of a fixed load with a variable resistor allows for the attainment of optimal efficiency across different frequency ranges.
- The rectenna under consideration exhibits a commendable conversion efficiency (CE) exceeding 65 % across the entirety of the five designated commercial frequency bands.

2. Proposed methodology

2.1. Proposed antenna

Rectennas, also known as rectifying antennas, are devices that integrate antenna components with rectifying circuits to capture and transform electromagnetic radiation into useable direct current (DC) electricity. Below is a concise outline of the rectenna design methodology.

- Antenna Design: The initial stage involves designing the individual component of the antenna. The process usually includes choosing an appropriate antenna type, such as dipole, patch, depending on the desired operating frequency and bandwidth specifications. The antenna should be engineered to effectively catch electromagnetic waves and transform them into electrical signals.
- Rectifier Design: The rectifier circuit converts the RF power to DC power.
- Rectifier with Matching Network: A matching network is commonly employed to optimise power transfer efficiency by aligning the impedance of the antenna with the rectifier circuit. This aids in guaranteeing that the utmost power is sent from the antenna to the rectifier.
- Optimisation: The design may be refined through iterative processes to enhance performance. Possible actions to improve efficiency and performance include modifying the antenna design, altering the rectifier circuit, or fine-tuning the matching network.
- Final Design: After the design has successfully met the necessary performance criteria, a final design is chosen, and the rectenna may be manufactured for practical purposes.

This section presents the proposal, simulation, and hardware design and testing of a conical antenna. The conical antenna under consideration exhibits operational capabilities spanning from 1.5 GHz to 4.65 GHz, and from 5.55 GHz to 7.85 GHz. These frequency bands are accompanied by respective bandwidths of 3.15 GHz and 2.3 GHz. In the realm of rectenna technology, the proposed system aims to cater to five distinct commercial bands, namely GSM 1.8 GHz, UTMS 2.1 GHz, 5G 3.5 GHz, 4.5 GHz, and 5.8 GHz 5G mid band (extended S-band and C band for 5G applications).

The simulation of the antenna entails the utilisation of diverse pyramidal structures, namely square, pentagonal, hexagonal, heptagonal, round, and conical. These pyramids serve as the radiating element, as depicted in Fig. 1. Fig. 2 portrays a visual representation of an antenna, showcasing both its top and bottom views in a three-dimensional format. The conical structure is affixed onto a substrate composed of FR-4 material, which exhibits lossy characteristics. Fig. 3 depicts the truncated conical antenna, serving as a visual aid to enhance comprehension regarding the fabrication process of the cone. The interior surface of the cone is constructed using a paper material, possessing a breadth of 1.6 mm and a dielectric constant of 2.31. The outer layer, on the other hand, is composed of copper foil with a thickness measuring 0.038 mm. Fig. 4 presents a comparative analysis of the (RL) displayed by an antenna featuring diverse configurations of radiating pyramids. The square pyramid antenna exhibits operational capabilities from 1.6 GHz to 2.11 GHz, 4 GHz–4.6 GHz, and 7.25 GHz–7.8 GHz. It is noteworthy that the BWs are 510 MHz, 200 MHz, and 550 MHz for the aforementioned frequency ranges, respectively. The minimum RL achieved is 15 dB at 1.8 GHz.

The pentagonal pyramid antenna exhibits operational capabilities

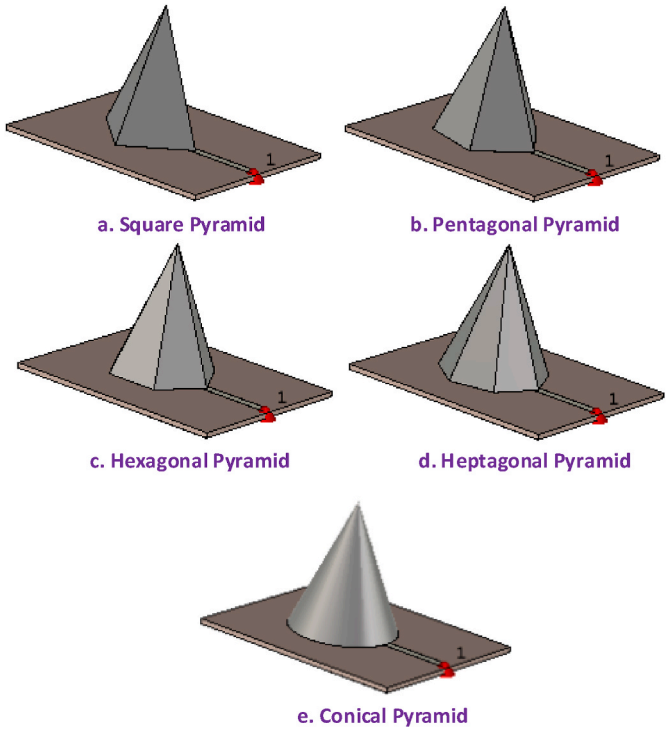

Fig. 1. Antenna with various pyramids.

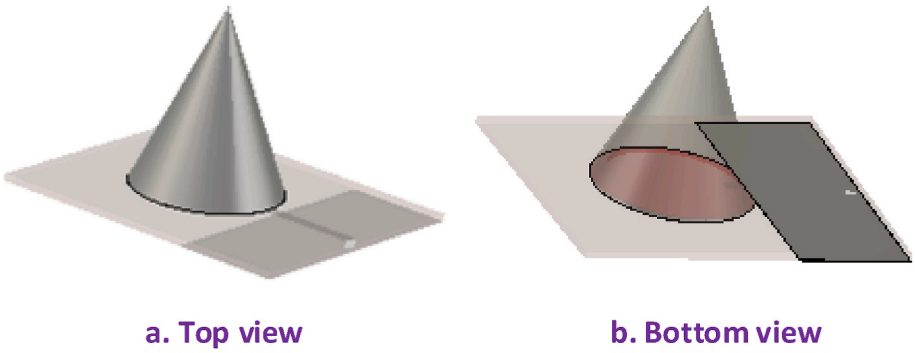

Fig. 2. 3D view of proposed antenna.

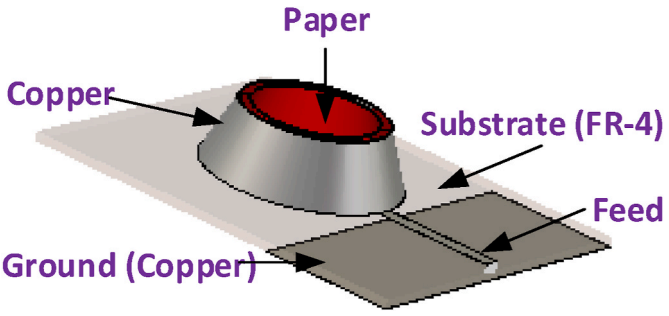

Fig. 3. Truncated view of conical antenna.

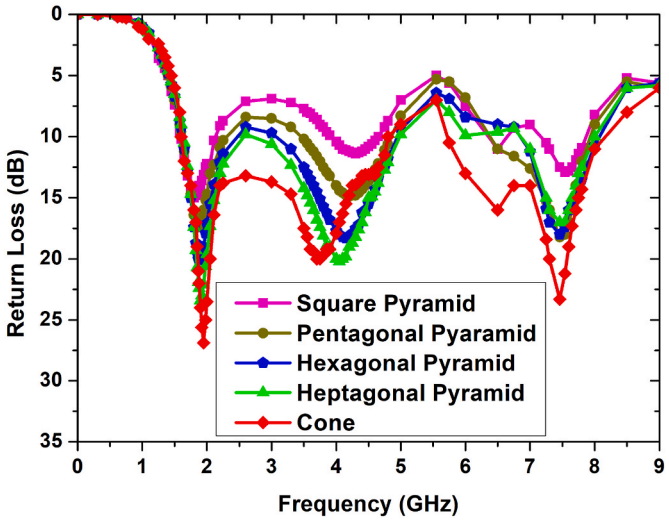

Fig. 4. Return Loss (RL) with various types of pyramids.

from 1.62 GHz to 2.25 GHz, 3.35 GHz–4.8 GHz, and 6.5 GHz–7.8 GHz, accompanied by corresponding bandwidths of 630 MHz, 1.45 GHz, and 1.3 GHz, correspondingly. The attained minimum RL is recorded at 17.4 dB within the frequency of 1.87 GHz. The hexagonal pyramid antenna exhibits operational frequencies spanning from 1.62 GHz to 2.35 GHz, 3.1 GHz–4.82 GHz, and 6.9 GHz–8 GHz, accompanied by corresponding bandwidths of 750 MHz, 1.72 GHz, and 1.1 GHz, correspondingly. The minimum achieved RL is measured to be 18.3 dB at 4.35 GHz. The antenna featuring a heptagonal pyramid structure exhibits operational capabilities from 1.65 GHz to 4.8 GHz, as well as 7 GHz–8 GHz, thereby offering a bandwidth of 3.15 GHz and 1 GHz, separately. The minimum achieved RL is quantified at 23.4 dB for 1.9 GHz. The conical pyramid antenna exhibits operational capabilities from 1.6 GHz to 4.8 GHz, as well as 5.7 GHz–8.2 GHz, thereby offering respective bandwidths of 3.2 GHz and 2.5 GHz. The minimum achieved RL is measured to be 26.9 dB (dB) at 1.95 GHz. These results are the achieved by simulation.

After successfully obtaining positive results with the conical pyramid antenna, subsequent efforts were undertaken to optimise said antenna by manipulating the dimensions of the cone, namely its height and radius. Initially height of the antenna remains constant while the radius is changed. The antenna, characterised by a conical radius of 12.5 mm, exhibits operational capabilities across three distinct frequency ranges: 1.6 GHz–2.2 GHz, 3.5 GHz–5 GHz, and 7.3 GHz–8 GHz. It is noteworthy that the bandwidth is 600 MHz, 700 MHz, and 1.5 GHz for each respective frequency range. The minimum value of the RL parameter was observed to be 19.6 dB at 4.35 GHz. The antenna, characterised by a conical radius of 15 mm, exhibits operational capabilities from 1.6 GHz to 4.8 GHz, 5.7 GHz–8.2 GHz, and offers corresponding bandwidths of 3.2 GHz and 2.5 GHz, separately. The minimum RL is quantified at 26.9 dB at1.95 GHz. The antenna, characterised by a conical radius measuring 17.5 mm, exhibits operational capabilities from 3.55 GHz to 4 GHz, 6.7 GHz–7.9 GHz, and affords BWs of 450 MHz and 1.2 GHz, correspondingly. The attained minimum RL is 32 dB, observed at 7.46 GHz. The antenna, characterised by a conical radius measuring 20 mm, operates within 3.2 GHz–3.65 GHz, 6.5 GHz–8 GHz, and offers bandwidths of 450 MHz and 1.5 GHz, correspondingly. The minimum achieved RL is 12.8 dB at a frequency of 7.8 GHz. Optimal outcomes are achieved when employing a cone radius measuring 15 mm. Nevertheless, it is noteworthy that the antenna's response remains almost same when subjected to height variations of both positive and negative 15 mm. The comparison of simulated RL for different cone radii is illustrated in Fig. 5.

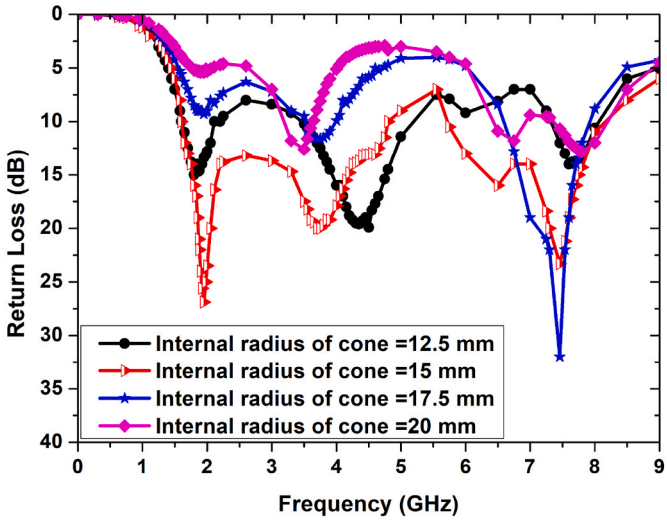

Fig. 5. RL with various sizes of conical pyramid.

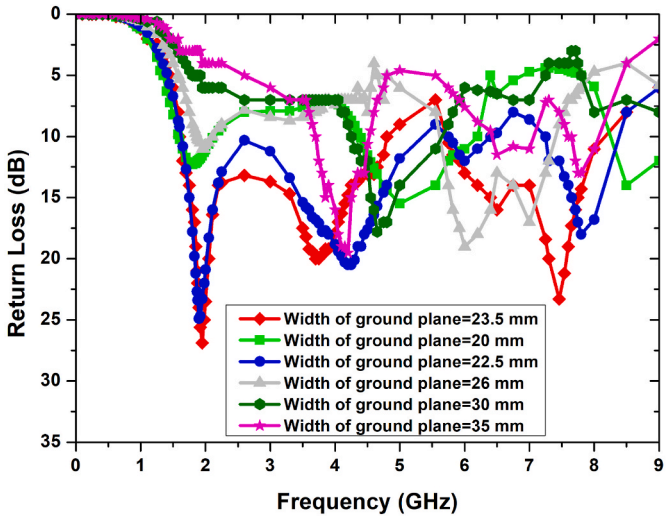

Fig. 6. RL with various sizes of ground plane.

The optimisation of the antenna is achieved through one more parameter that is the utilisation of the ground plane's width (GPW) (see Fig. 6). The antenna under consideration exhibits a GPW of 20 mm and operates from 1.6 GHz to 2.11 GHz and 4.4 GHz–6.2 GHz. It is noteworthy that this antenna offers a bandwidth of 510 MHz and 1.8 GHz for the aforementioned frequency ranges, respectively. The minimum RL achieved is quantified at 15.5 dB when operating at 5 GHz. The antenna under consideration exhibits a ground plane width (GPW) of 22.5 mm, enabling its functionality across three distinct frequency ranges. Specifically, it operates from 1.65 GHz to 5 GHz, 5.75 GHz–6.4 GHz, and 7.25 GHz–8.2 GHz. Each of these frequency ranges offers a corresponding bandwidth of 3.35 GHz, 350 MHz, and 950 MHz, respectively. The minimum RL achieved in this particular scenario is measured at 24.9 dB at a frequency of 1.9 GHz. The antenna under consideration possesses a ground plane width (GPW) of 23.5 mm, enabling its functionality from 1.6 GHz to 4.8 GHz, 5.7 GHz–8.2 GHz, thereby offering a BWs of 3.2 GHz and 2.5 GHz, correspondingly. The minimum achieved RL is measured to be 26.9 dB at 1.95 GHZ. The antenna under consideration exhibits a ground plane width (GPW) of 26 mm, enabling its operation from 1.87 GHz to 2.11 GHz, 5.6 GHz–7.4 GHz, with corresponding BWs of 3.49 GHz and 1.9 GHz, respectively. The minimum achieved RL is measured to be 19 dB at 6 GHz. The antenna under consideration possesses a gain-bandwidth product (GPW) of 30 mm, effectively operating from 4.25 GHz to 5.6 GHz. It is noteworthy that this antenna exhibits a BW of 2.35 GHz. The minimum achieved level of RL is 17.8 dB at 4.65 GHz. The antenna under consideration exhibits a gain-bandwidth product (GPW) of 35 mm, operating from 6.42 GHz to 7.1 GHz, thereby present a bandwidth of 680 MHz. The least achieved RL is 11 dB at 7 GHz.

Optimal outcomes are achieved through the utilisation of a conical pyramid as a radiating structure, characterised by a radius of 15 mm and a GPW of 23.5 mm. After achieving successful simulated results, the fabrication phase of the antenna is started. The topological depiction of the made-up antenna is presented in Fig. 7 (a), while the lateral perspective is illustrated in Fig. 7 (b), and the posterior view is exhibited in Fig. 7 (c). The antenna that has been artificially created is subjected to testing using a spectrum analyzer. The resulting reflection coefficient (RL) is then compared among the simulated and measured values, as depicted in Fig. 8. The results obtained from the simulated reinforcement learning (RL) indicate that the antenna exhibits resonance from 1.6 GHz to 4.8 GHz, as well as 5.7 GHz–8.2 GHz. Moreover, the antenna demonstrates a BWs of 3.2 GHz and 2.5 GHz for the aforementioned frequency ranges, respectively. The obtained results indicate that the measured resonance from 1.5 GHz to 4.65 GHz and 5.55 GHz–7.85 GHz,

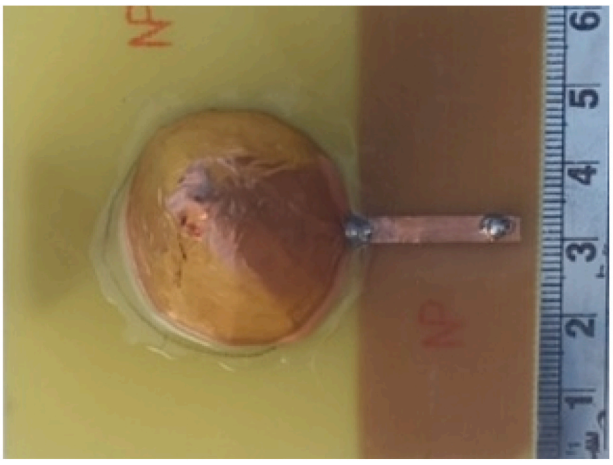

(a) Top view of designed antenna

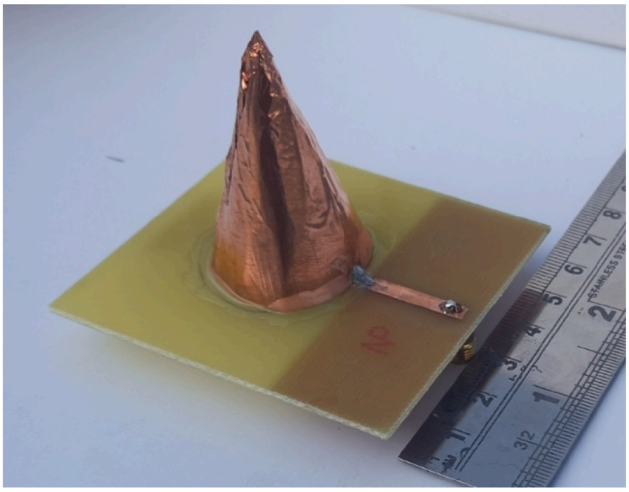

(b) Side view of designed antenna

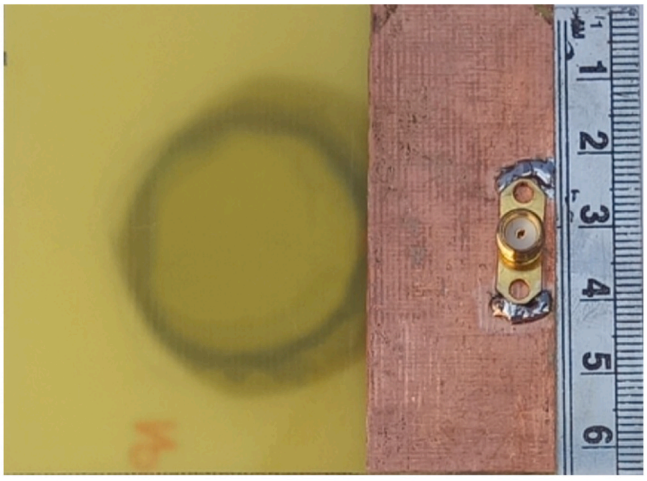

(c) Back side of printed antenna

Fig. 7. (a) Top view of designed antenna. (b) Side view of designed antenna. (c) Back side of printed antenna.

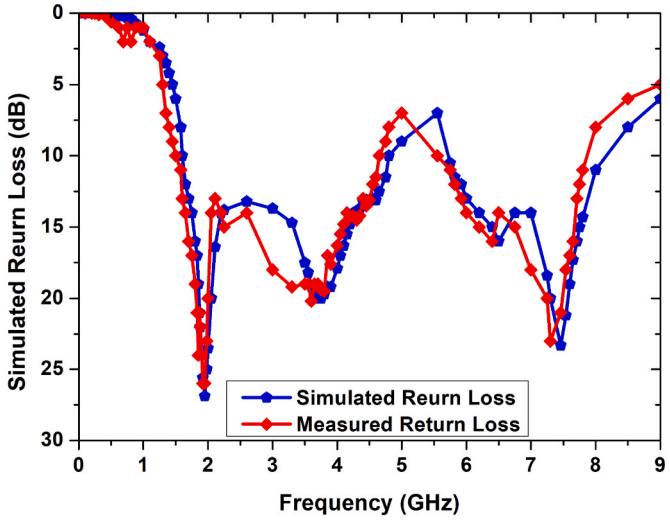

Fig. 8. Simulated and measured returnloss comparison.

with corresponding BWs of 3.15 GHz and 2.3 GHz, respectively. A discernible inclination towards the left has been observed in the measured RL, which can be attributed to the inherent variability in paper quality and thickness.

The gain is assessed for various frequencies, specifically 1.8 GHz, 2.1 GHz, 3.5 GHz, 4.5 GHz, and 5.8 GHz, with an angular orientation of $\theta = 90^\circ$ and $\varphi = 90^\circ$. The plot in Fig. 9 (a), 9 (b), 9 (c), 9 (d), and 9 (e) illustrates the fluctuation of gain within these frequency bands at different angles. The maximum simulated and measured gain (SMG) at a frequency of 1.8 GHz is found to be 2 dBi, and 2.2 dBi observed specifically in the directions of 90° and 270°. At 2.1 GHz the maximum SMG is 2.4 dBi. and 2.5 dBi in the specific directions of 95° and 265°. At 3.5 GHz SMG is 3.3 dBi and 3.5 dBi when oriented towards 130° and 230°. The maximum SMG at 4.5 GHz isis 5.3 dBi and 5.1 dBi when the antenna is oriented towards 135° and 225°. The maximum SMG at 5.8 GHz is 4.7 dBiand 4.5 dBi when oriented towards 150° and 210°.

2.2. Rectifier design

The present study introduces a novel design of a dual ultra-wideband rectenna for S and C bands. The proposed rectenna exhibits the capability to efficiently harvest energy from 1.5 GHz to 4.65 GHz, as well as from 5.55 GHz to 7.85 GHz. The respective BWs for these frequency ranges are measured to be 3.15 GHz and 2.3 GHz. The proposed rectenna system is designed to cater to a selection of five prominent commercial frequency bands, namely GSM 1.8 GHz, UTMS 2.1 GHz, 5G 3.5 GHz, 4.5 GHz, and 5.8 GHz 5G mid band (extended S-band and C band for 5G applications). The rectenna system is comprised of an antenna and a high frequency rectifier. The selection of a compact conical antenna is predicated upon its inherent broadband characteristics, which render it suitable for the utility of RF emanating from diverse frequency bands, as expounded upon in the preceding section. For the purpose of rectification, a solitary HSMS 2850 Schottky diode has been chosen. The rectifier circuit depicted in Fig. 10, in the absence of an IMN, yields a significantly diminished conversion efficiency (CE).

In order to enhance the CE, a rectifier circuit has been devised, incorporating a three branch pi-impedance matching network (IMN). Additionally, a DC combining method has been implemented to enable the connection among the antenna and the rectifier. To evaluate the CE, it is imperative to measure the powers of both the input and output. Subsequently, the conversion efficiency can be ascertained by employing the equation provided [30].

$$\eta c = \frac{Pout}{Pin} x100\% \quad (1)$$

where: P_{out} = Output DC power, ηc = Conversion efficiency, P_{in} = Input RF power.

Multiple impedance matching networks (IMNs) have been identified in the literature, including the Pi-Network, L-Network, and T-Network, as referenced in Ref. [31]. The process of achieving impedance matching between a 50 Ω system and the HSMS2850 impedance is accomplished by employing the Smith chart on ADS 2020 software. The utilisation of the DC combining technique is implemented to amalgamate the outputs originating from the two branches of the Integrated Multimodal Network. The rectifier circuit illustrated in Fig. 11 showcases the incorporation of an Integrated Magnetic Nanoparticle (IMN). After the successful integration of these various branches, the circuit undergoes subsequent optimisation and simulation procedures utilising a harmonic balance (HB) method within the ADS 2020 software platform.

The measured values of the inductance elements for the Integrated Magnetic Nanodevice (IMN) are as follows: L1 = 26.07 nH, L2 = 17.7117 nH, L3 = 5.16 nH, L4 = 2.588 nH, L5 = 5.855 nH, L6 = 1.96 nH, L7 = 11.31 nH, L8 = 6.88 nH, and L9 = 14.19 nH. The given values for the capacitors are as follows: C1 = 0.513 pF, C2 = 0.277 pF, C3 = 5.1454 pF, C4 = 0.0001 pF, C5 = 0.4 pF, C6 = 0.665 pF, C7 = 1.06 pF, C8 = 1.599 pF, and C9 = 0.2699 pF. In addition, a by-pass capacitor of 0.005 nF has been selected. The lumped parameters are converted into equivalent microstrip lines, and subsequently, the circuit is simulated and optimised utilising ADS 2020. Fig. 15 illustrates the frontal perspective of the fabricated rectifier. In contrast to a fixed value load resistor, a variable resistor is utilised, as depicted in Fig. 15, to enable the manipulation of the load and achieve optimal CE across different frequencies.

3. Rectifier results and discussion

The current investigation involves an examination of the suggested rectifier in relation to the five important commercial frequency bands, specifically GSM 1.8 GHz, UTMS 2.1 GHz, 5G 3.5 GHz, 4.5 GHz, and 5.8 GHz 5G mid bands. The simulation encompasses a range of load resistances, specifically 200 Ω, 500 Ω, 1000 Ω, 1500 Ω, 2200 Ω, and 2600 Ω. Furthermore, the simulation is conducted across a range of IPLs spanning from −20 dBm to 10 dBm. Fig. 13 depicts the graphical representation of the fluctuation in CE at a frequency of 1.8 GHz. The coefficient of efficiency (CE) was ascertained at different IPLs utilising a 200 Ω load. At an IPL of −20 dBm, the CE was determined to be 8 %. At an IPL of −15 dBm, the CE was determined to be 12 %. In a comparable manner, when considering an IPL of −10 dBm, the CE was observed to be 16.3 %. At an IPL of −5 dBm, the CE exhibited an increment to 20 %. Similarly, when the IPL was adjusted to 0 dBm, the CE demonstrated a further enhancement, reaching 21.8 %. Under identical load conditions, the CE achieved at an IPL of 5 dBm is measured to be 23 %. Conversely, when the IPL is increased to 10 dBm, the CE is observed to decrease to 20 %.

The CE was assessed at different IPLs while utilising a 500 Ω load. Specifically, when the IPL was measured at −20 dBm, the corresponding CE was determined to be 14 %. Upon conducting an experiment with IPL of −15 dBm, it was determined that the CE reached a value of 23.2 %. In a comparable manner, when considering an IPL of −10 dBm, the CE was observed to be 16.331.6 %. At an IPL of −5 dBm, the CE exhibited an increase to 37.8 %. Similarly, when the IPL was adjusted to 0 dBm, the CE demonstrated a further increment to 42 %. Under identical load conditions, the CE achieved at an IPL of 5 dBm is determined to be 44.5 %. Conversely, when the IPL is increased to 10 dBm, the CE diminishes to 16 %. The CE was assessed at different IPLs while utilising a 1000 Ω load. Notably, at an IPL of −20 dBm, the CE was empirically determined to be 19.7 %. The investigational outcomes designate that at an IPL of −15 dBm, the CE was determined to be 32.9 %. In a similar vein, when considering an IPL of −10 dBm, the CE was observed to be 44.5 %. At an IPL of −5 dBm, the CE exhibited an increase to 53.2 %. Subsequently, at

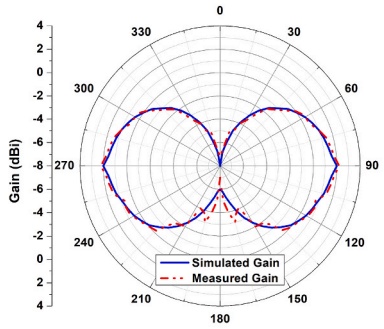

(a) Gain variation at 1.8 GHz

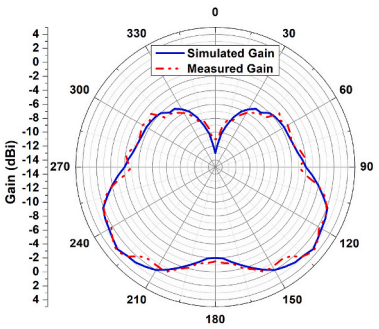

(c) Gain variation at 3.5 GHz

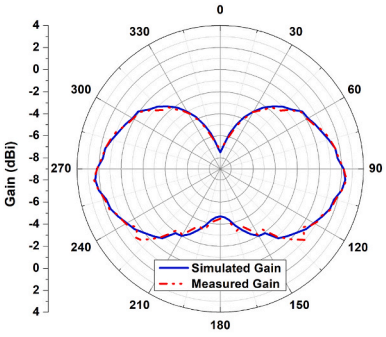

(b) Gain variation at 2.1 GHz

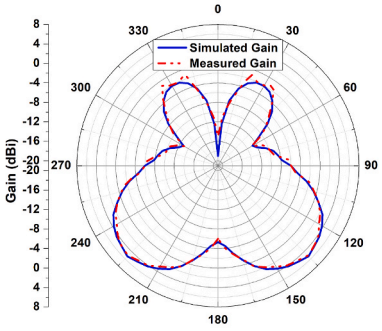

(d) Gain variation at 4.5 GHz

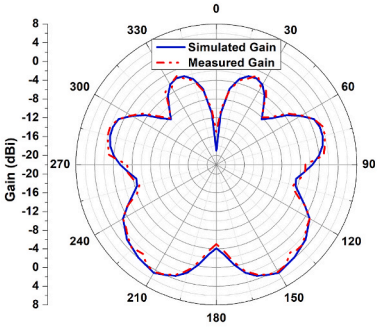

(e) Gain variation at 5.8 GHz

Fig. 9. (a) Gain variation at 1.8 GHz. (b) Gain variation at 2.1 GHz. (c) Gain variation at 3.5 GHz. (d) Gain variation at 4.5 GHz. (e) Gain variation at 5.8 GHz.

an IPL of 0 dBm, the CE was observed to reach 60.7 %. Under the condition of a consistent load, the CE achieved at an IPL of 5 dBm is measured to be 60.2 %. Conversely, when the IPL is increased to 10 dBm, the CE decreases to 32 %.

The CE was assessed across IPLs while utilising a 1500 Ω load. Specifically, when the IPL was set to −20 dBm, the CE was observed to be 22.3 %. At an IPL of −15 dBm, the CE was determined to be 37.4 %. In a similar vein, it is worth noting that at an IPL of −10 dBm, the CE was measured to be 51 %. At an IPL of −5 dBm, the CE exhibited an increase to 64.7 %. Similarly, when the IPL was raised to 0 dBm, the CE was observed to reach a value of 64.5 %. Under the condition of a consistent load, the CE achieved at an IPL of 5 dBm is measured to be 57.3 %. Conversely, when the IPL is increased to 10 dBm, the CE is observed to be 21 %. The CE was assessed at IPLs using a load of 2200 Ω. Specifically, when the IPL was measured at −20 dBm, the CE was determined to be 22.8 %. At an IPL of −15 dBm, the CE was determined to be 36 %. In a comparable fashion, when considering an IPL of −10 dBm, the CE was observed to be 60.3 %. At an IPL of −5 dBm, the CE exhibited an increase to 66.3 %. Similarly, when the IPL was adjusted to 0 dBm, the CE was observed to reach a value of 59.2 %. Under identical load conditions, the CE achieved at an IPL of 5 dBm is measured to be 45.6 %. Conversely, when the IPL is increased to 10 dBm, the CE is observed to be 2 %.

The CE) was measured at IPLs using a 2600 Ω load. Specifically, at an IPL of −20 dBm, the CE was determined to be 24.1 %. At an IPL of −15 dBm, the CE was determined to be 41.2 %. In a comparable manner, when considering an IPL of −10 dBm, the CE was determined to be 60.363 %. At an IPL of −5 dBm, the CE exhibited a notable increase, reaching a value of 65 %. Similarly, when the IPL was raised to 0 dBm, the CE was observed to attain a slightly lower value of 55.4 %. Under identical conditions, the CE achieved at an IPL of 5 dBm is measured to be 39.1 %. Conversely, when the IPL is increased to 10 dBm, the CE decreases significantly to 4 %. The maximum achieved CE at a frequency

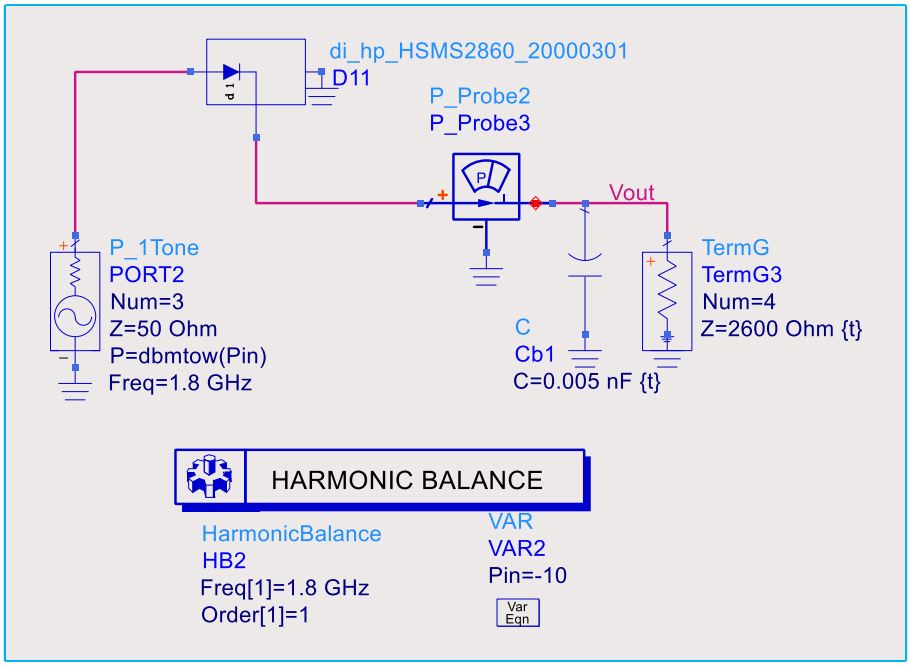

Fig. 10. Rectifier without matching network.

of 1.8 GHz is 67 %, as determined by an IPL of −7 dBm and a load of 1500 Ω. Fig. 14 depicts the graphical representation of the fluctuation in CE at a frequency of 2.1 GHz. The maximum CE attained when utilising a 200 Ω load is 18 % at an IPL of 10 dBm. Similarly, the highest CE attained with a 500 Ω load is 36.4 % at an IPL of 10 dBm. The extreme CE achieved when a 1000 Ω load is applied is measured to be 55.3, accompanied by an IPL of 7 dBm. The CE was assessed across multiple IPLs while utilising a 1500 Ω load. Notably, at an IPL of −10 dBm, the CE was observed to be 7 %. At an IPL of −5 dBm, the CE exhibited a notable increase, reaching 21 %. Similarly, when the IPL was raised to 0 dBm, the CE experienced further enhancement, reaching a commendable 45 %. Under identical conditions, the CE achieved at an IPL of 5 dBm is 53 %, whereas at an IPL of 10 dBm, the CE is observed to be 20 %. The supreme CE achieved when a 2200 Ω load is applied is quantified as 56.4, accompanied by an IPL of 7 dBm. The extreme value of the CE attained when a 2600 Ω load is connected is 47.6, while the IPL is measured at 4 dBm. The maximum simulated CE attained at a frequency of 2.1 GHz is 63 %, with an IPL of 4 dBm and a load resistance of 1500 Ω.

Fig. 15 depicts the fluctuation of CE at 3.5 GHz. The highest CE attained when utilising a 200 Ω load is 52 % at an IPL of 10 dBm. Conversely, the extreme CE attained with a 500 Ω amounts to 63 % at the same IPL of 10 dBm. The maximum achieved CE with a resistance of 1000 Ω is determined to be 74.8 %, while operating at an IPL of 6 dBm. The CE was assessed at different IPLs while utilising a 1500 Ω load. Notably, at an IPL of −10 dBm, the CE was observed to be 15 %. At an IPL of −5 dBm, the CE exhibited an increase to 35 %. Similarly, at an IPL of 0 dBm, the CE demonstrated a further enhancement, reaching 66.8 %. Under identical load conditions, the CE achieved at an IPL of 5 dBm is 66.2 %. Conversely, when the IPL is increased to 10 dBm, the CE is observed to be 22 %. The maximum CE attained when operating with a 2200 Ω load is 71.4 %, observed at an IPL of 2 dBm. The maximum CE attained when operating with a 2600 Ω load is recorded as 68.8 %, corresponding to an IPL of 2 dBm. The maximum attainable efficiency achieved at a frequency of 3.5 GHz amounts to 77.5 %, given an IPL of 4 dBm and a resistance of 1500 Ω.

Fig. 16 illustrates the fluctuation of the CE characteristics at 4.5 GHz. The CE was assessed at multiple IPLs utilising a 200 Ω load. Notably, at an IPL of −10 dBm, the CE was measured to be 13 %. At an IPL of −5 dBm, the CE exhibited an increase to 36.5 %. Subsequently, when the IPL was raised to 0 dBm, the CE demonstrated a further enhancement, reaching 64.6 %. Under identical load conditions, the CE achieved at IPL of 5 dBm is 39.5 %, whereas at an IPL of 10 dBm, it is 13 %. The maximum CE attained when operating with a 500 Ω load is 44 % at an IPL of 10 dBm. The maximum CE attained when a 1000 Ω load is employed is 32 %, corresponding to an IPL of 2 dBm. The supreme CE attained when a 1500 Ω load is applied is 19.4 % at an IPL of −3 dBm. The maximum CE attained when a 2200 Ω load is employed amounts to 18.7 %, corresponding to an IPL of 8 dBm. The maximum CE attained when operating with a 2200 Ω load is recorded as 17.2 %, corresponding to an IPL of 8 dBm. The maximum CE achieved at a frequency of 4.5 GHz is 70 %. This result was obtained under the conditions of an IPL of 2 dBm and a load impedance of 200 Ω.

The graphical representation in Fig. 17 illustrates the fluctuation of CE at 5.8 GHz. The extreme CE attained when utilising a 200 Ω load is 57 % at an IPL of 10 dBm. The CE was assessed across different IPLs while utilising a 500 Ω load. Notably, at an IPL of −10 dBm, the CE was observed to be 8 %. At an IPL of −5 dBm, the CE exhibited an increment to 28 %. Similarly, when the IPL was raised to 0 dBm, the CE experienced a subsequent rise to 51 %. Under identical load conditions, the CE achieved at an IPL of 5 dBm is measured to be 66.1 %. Conversely, when the IPL is increased to 10 dBm, the CE decreases to 57 %. The extreme CE attained when a 1000 Ω load is employed is 62.7 %, observed at an IPL of 6 dBm. The peak CE attained when operating with a 1500 Ω load is recorded as 52.4 % when the IPL is set at 5 dBm. The peak CE attained when a 2200 Ω load is utilised is 43.1 %, corresponding to an IPL of 5 dBm. The peak CE attained when utilising a 2600 Ω load is 39 % with an IPL of 3 dBm. The maximum achieved CE at a frequency of 5.8 GHz is recorded as 71.3 percent. This result is accompanied by an IPL of 9 dBm and a load impedance of 200 Ω (Ω).

The graphical representation in Fig. 18 depicts the fluctuation of the output voltage in relation to different power levels and load resistances. The observed maximum output voltages, corresponding to different load resistances of 200 Ω, 500 Ω, 1000 Ω, 1500 Ω, 2200 Ω, and 2600 Ω, are measured to be 0.62 V, 1.5 V, 1.819 V, 1.8 V, and 1.8 V, correspondingly.

The rectifier that has been fabricated is illustrated in Fig. 12, and it has undergone testing utilising a Vector Network Analyzer (VNA). The rectenna system was evaluated within an ambient environment, yielding a maximum output voltage of 125 mV. Fig. 19 provides a graphical

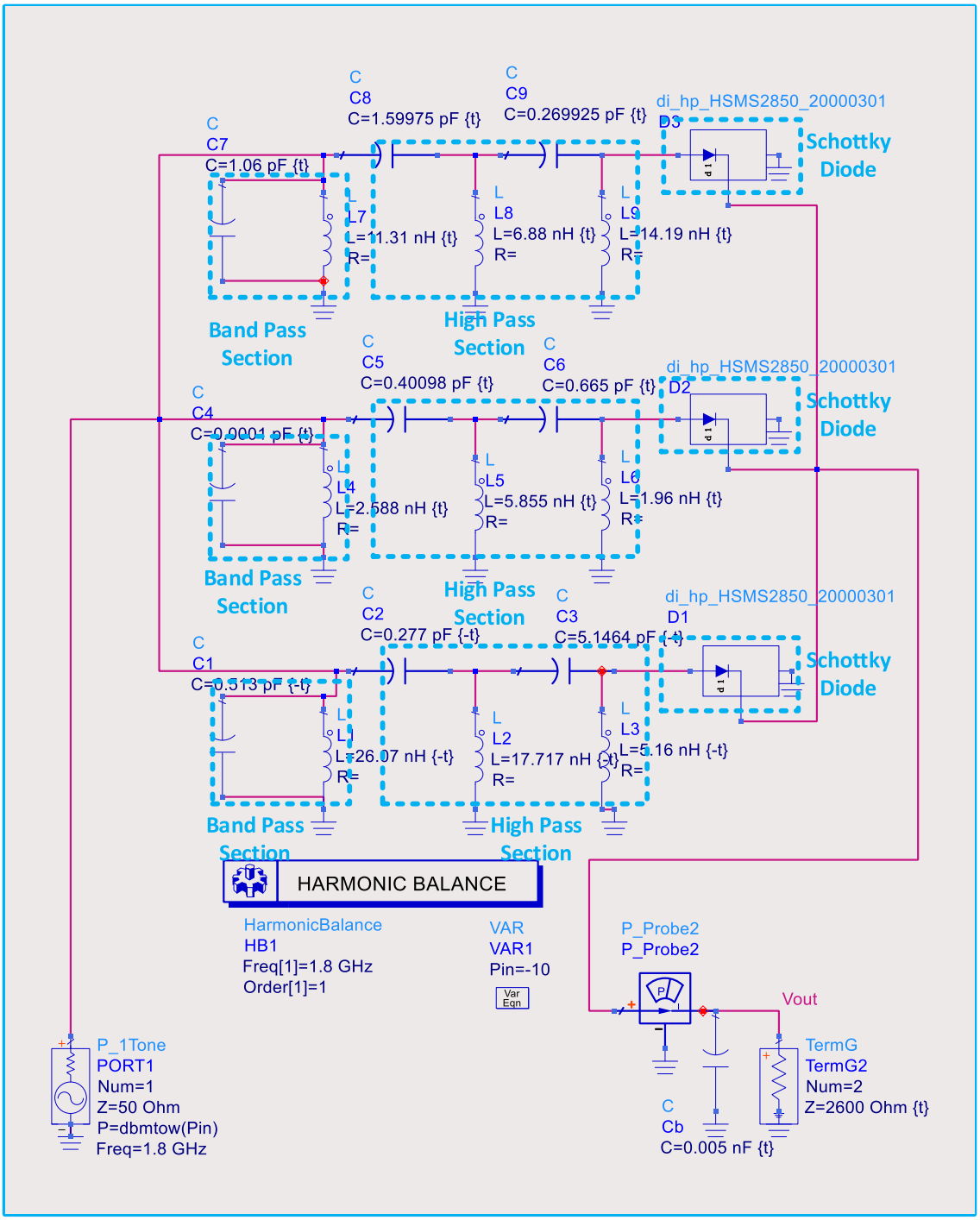

Fig. 11. Rectifier circuit with matching.

illustration of the comparison between the simulated and measured CE for different planned frequency ranges. At a frequency of 1.8 GHz, the highest recorded CE was 67.5 % while the IPL was −6 dBm. The CE values obtained at various levels of IPL are as follows: at −20 dBm, the CE is 24 %; at −15 dBm, the CE is 40 %; at −10 dBm, the CE is 62.8 %; at −5 dBm, the CE is 65 %; at 0 dBm, the CE is 58 %; and at 5 dBm, the CE is 43 %. At a frequency of 2.1 GHz, the highest recorded CE was 65 % when the IPL was 4 dBm. The CE values obtained at different power levels are as follows: at −5 dBm, the CE is 17 %; at 0 dBm, the CE is 41 %; and at 5 dBm, the CE is 56 %. At a frequency of 3.5 GHz, the highest recorded CE was 77 % when the IPL reached 4 dBm. The CE values obtained at different power levels are as follows: at −5 dBm, the CE is 36 %; at 0 dBm, the CE is 64 %; and at 5 dBm, the CE is 65 %. At a frequency of 4.5 GHz, the highest recorded CE is 70 % when the IPL is 2 dBm. The CE values for different power levels are as follows: at −5 dBm, the CE is 37 %; at 0 dBm, the CE is 63 %; and at 5 dBm, the CE is 58 %. At a frequency of 5.8 GHz, the highest recorded CE is 71 % when the IPL is 9 dBm. The efficiency of the system, as measured by the CE, decreases as the power level decreases. At an IPL of −5 dBm, the CE is 28 %. At 0 dBm, the CE increases to 52 %, and at 5 dBm, the CE further increases to 65 %. The observed highest CE across all frequencies exceeds 65 %.

Table 1 displays a comparison analysis between the rectifier that has been presented and the rectifiers that are already designed by researchers.

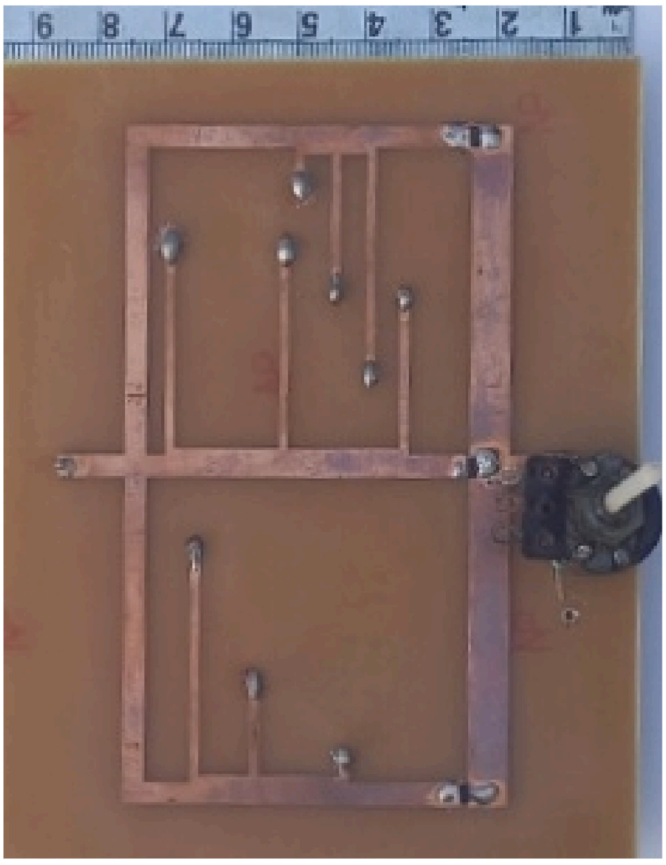

Fig. 12. Fabricated rectifier's front side.

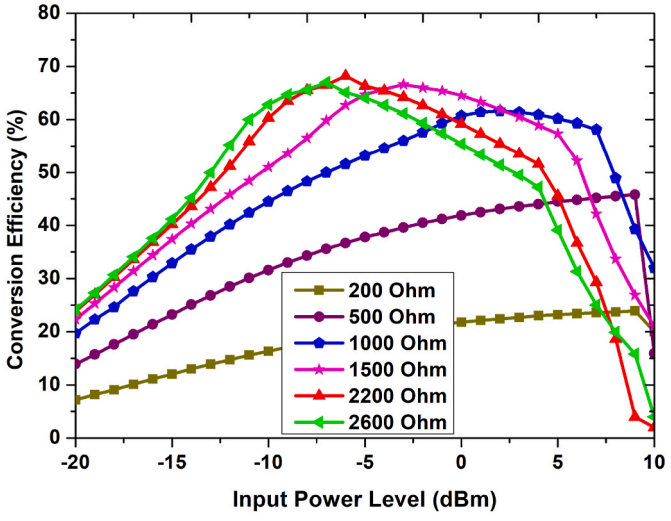

Fig. 13. Conversion efficiency at 1.8 GHz.

4. Conclusion

The design of a dual ultra-wideband rectenna is presented for the purpose of RF energy harvesting from the S and C bands. The suggested rectenna is specifically designed to capture energy from 1.5 GHz to 4.65 GHz and 5.55 GHz–7.85 GHz, with respective bandwidths of 3.15 GHz and 2.3 GHz. The proposed rectenna has been specifically developed to function within the frequency ranges of five distinct commercial bands. The frequency bands utilised by several generations of mobile communication technologies are as follows: GSM operates at 1.8 GHz, UTMS

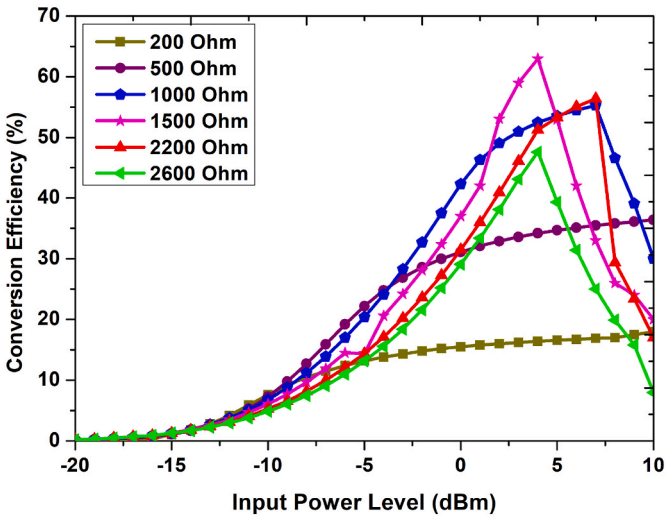

Fig. 14. Conversion efficiency at 2.1 GHz.

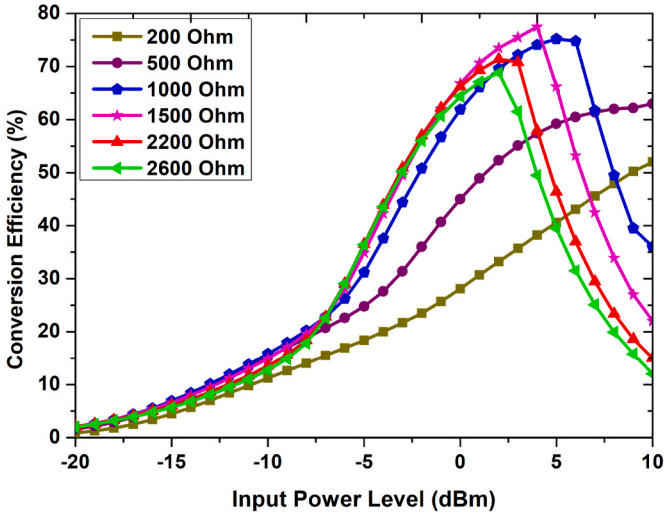

Fig. 15. Conversion efficiency at 3.5 GHz.

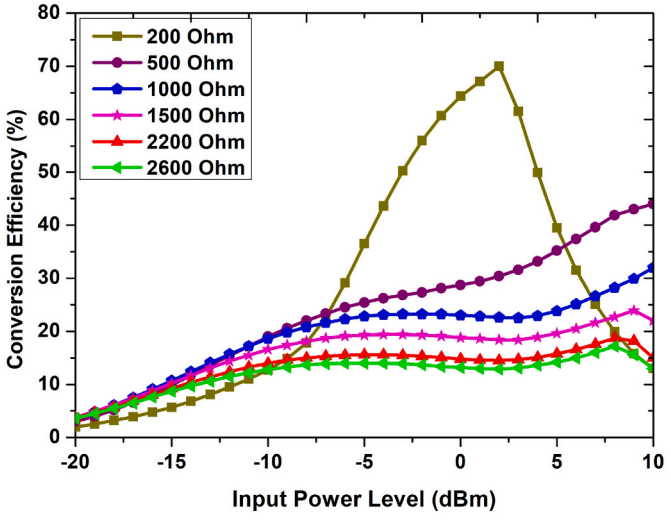

Fig. 16. Conversion efficiency at 4.5 GHz.

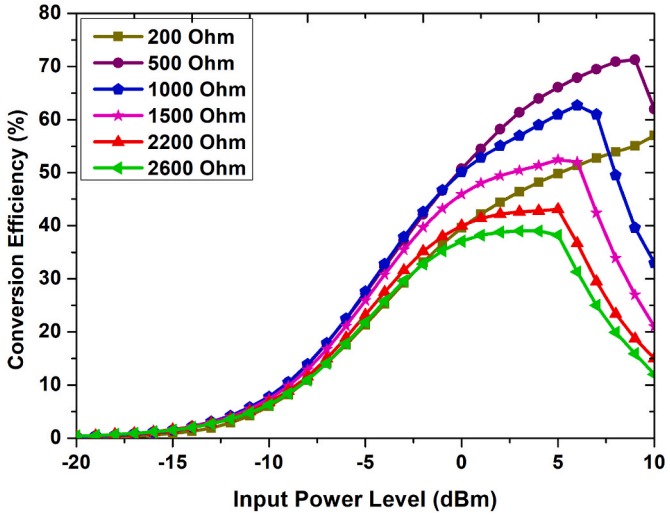

Fig. 17. Conversion efficiency at 5.8 GHz.

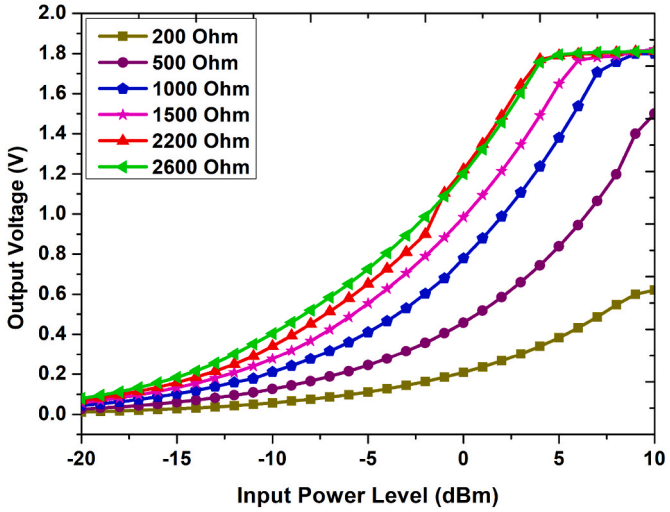

Fig. 18. Output voltage.

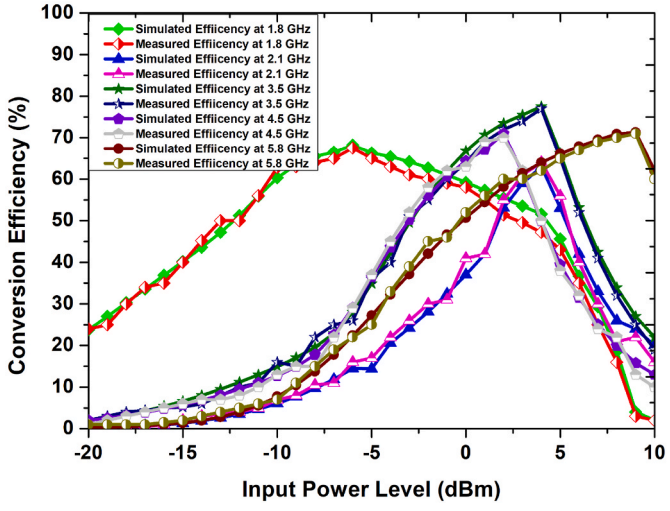

Fig. 19. Simulated and measured CE.

Table 1
Comparison with previous work.

Ref.	Frequency band (GHz)	Schottky diode used	Efficiency (%) @ Pin
[02]	0.9–1.9	HSMS 2850	78@6.5 dBm
[13]	2.45	HSMS2860	85.7@16 dBm
[23]	0.9	HSMS2852	33.7@-10dBm
	1.8		21.8@-10dBm
	2.45		20@-10dBm
[27]	0.9–3	HSMS 2850	73.4@3dBm
[28]	3.1–8	SMS7630	69@-10dBm
[30]	2.06–5.0	HSMS 2852	52@0dBm
This Paper	1.5–4.65, 5.55–7.85	HSMS 2850	77@4 dBm 71 %@2 dBm

operates at 2.1 GHz, and 5G operates at many frequencies including 3.5 GHz, 4.5 GHz, and 5.8 GHz. Additionally, 5G mid band encompasses the extended S-band and C band frequencies, which are specifically allocated for 5G purposes. A small conical antenna is designed to exhibit broadband properties. To boost the conversion efficiency (CE), a method using a three-line IMN and DC combining is employed between the antenna and rectifier. The rectenna under consideration is designed to operate across five distinct frequency bands. In all of these frequency bands, the conversion efficiency (CE) exceeds 65 %. As a result, the rectenna demonstrates an elevated level of output power, rendering it well-suited for the purpose of supplying energy to low-power electronic equipment. The rectenna was subjected to testing within the surrounding environment, resulting in an output voltage of 125 mV. The rectenna under consideration has the potential to be employed for the purpose of supplying power to a range of low-power sensors. A supercapacitor can be employed to store direct current (DC) power for further utilisation.

CRediT authorship contribution statement

Shailendra Singh Ojha: Writing – review & editing, Writing – original draft, Visualization, Validation, Resources, Methodology, Investigation, Formal analysis, Data curation, Conceptualization. **Jai Kumar Sharma:** Writing – review & editing, Writing – original draft, Visualization, Validation, Methodology, Investigation. **Bhupendra Dhakad:** Writing – review & editing, Writing – original draft, Visualization, Validation, Methodology. **Sateesh Kumar:** Writing – review & editing, Writing – original draft, Visualization, Validation. **Neeraj Sharma:** Writing – review & editing, Writing – original draft, Visualization, Validation, Methodology. **Anuj Kumar Pandey:** Writing – review & editing, Writing – original draft, Methodology, Conceptualization. **S.M. Mozammil Hasnain:** Writing – review & editing, Writing – original draft, Validation, Methodology, Investigation. **Sandeep Kumar:** Conceptualization, Data curation, Formal analysis, Visualization, Writing – original draft, Writing – review & editing. **Rahul Kumar:** Conceptualization, Formal analysis, Methodology, Visualization, Writing – original draft, Writing – review & editing.

Declaration of competing interest

The authors declare that they have no known competing financial interests or personal relationships that could have appeared to influence the work reported in this paper.

Data availability

Data will be made available on request.

References

[1] Rasool Keshavarz, Negin Shariati, Highly sensitive and compact quad-band ambient RF energy harvester, IEEE Trans. Ind. Electron. 69 (4) (2021) 3609–3621.

[2] Shailendra Singh Ojha, P.K. Singhal, Vandana Vikas Thakare, Dual-band rectenna system for biomedical wireless applications, Measurement: Sensors (2022) 100532.
[3] Shailendra Singh Ojha, et al., 2-GHz dual diode dipole rectenna for wireless power transmission, Int J Microw Opt Technol 8 (2013) 2.
[4] Wei Huang, et al., A novel 24 GHz circularly polarised metasurface rectenna, IET Microw., Antennas 17 (6) (2023) 419–426.
[5] Shailendra Singh Ojha, P.K. Singhal, Vandana Vikas Thakare, Triple-wideband antenna for RF energy harvesting, in: International Conference on Communication, Networks and Computing, Springer Nature Switzerland, Cham, 2022.
[6] Shailendra Singh Ojha, et al., Dual-band antenna and low pass filter design for wireless energy harvesting, in: International Conference on Communication, Networks and Computing, Springer Nature Switzerland, Cham, 2022.
[7] J.J. Estrada-López, A. Abuellil, A. Costilla-Reyes, M. Abouzied, S. Yoon, E. Sánchez Sinencio, A fully integrated maximum power tracking combiner for energy harvesting IoT applications, IEEE Trans. Ind. Electron. 67 (4) (2020) 2744–2754.
[8] A. Shareef, W.L. Goh, S. Narasimalu, Y. Gao, A rectifier-less AC–DC interface circuit for ambient energy harvesting from low-voltage piezoelectric transducer array, IEEE Trans. Power Electron. 34 (2) (2019) 1446–1457.
[9] K. Ali, D.J. Rogers, An orientation-independent multi-input energy harvesting wireless sensor node, IEEE Trans. Ind. Electron. 68 (2) (2021) 1665–1674.
[10] N. Cansiz, D. Altinel, G.K. Kurt, Efficiency in RF energy harvesting systems: a comprehensive review, Energy 174 (2019) 292–309.
[11] F. Ünlü, L. Wawrla, Energy Harvesting Technologies for IoT Edge Devices, Helbling Technik AG, 2018.
[12] V. Marian, B. Allard, C. Vollaire, J. Verdier, Strategy for microwave energy harvesting from ambient field or a feeding source, IEEE Trans. Power Electron. 27 (11) (2012) 4481–4491.
[13] Shailendra Singh Ojha, Pramod Kumar Singhal, Vandana Vikas Thakare, Highly efficient dual diode rectenna with an array for RF energy harvesting, Wireless Pers. Commun. (2023) 1–22.
[14] Chayma Bahhar, Chokri Baccouche, Hedi Sakli, A novel 5g rectenna for iot applications, in: 2020 20th International Conference on Sciences and Techniques of Automatic Control and Computer Engineering (STA), IEEE, 2020.
[15] Trung Dung Ha, Liang Zhu, Pai-Yen Chen, A low-cost wide-angle multi-beam coverage Bruce rectennas for energy harvesting applications, in: 2022 IEEE International Symposium on Antennas and Propagation and USNC-URSI Radio Science Meeting (AP-S/URSI), IEEE, 2022.
[16] D. Lee, T. Kim, S. Kim, K. Byun, K. Kwon, A CMOS rectifier with 72.3% RF-toDC conversion efficiency employing tunable impedance matching network for ambient RF energy harvesting, in: International SoC Design Conference (ISOCC), Daegu, Korea (South), 2018.
[17] N. Cansiz, D. Altinel, G.K. Kurt, Efficiency in RF energy harvesting systems: a comprehensive review, Energy 174 (2019) 292–309.
[18] A. Okba, S. Charlot, P. Calmon, A. Takacs, H. Aubert, Multiband rectenna for microwave applications, in: IEEE Wireless Power Transfer Conference (WPTC), Aveiro, 2016.
[19] N. Shariati, W.S.T. Rowe, K. Ghorbani, Highly sensitive FM frequency scavenger integrated in building materials, in: European Microwave Conference, EuMC), Paris, 2015.
[20] Jiunn-Kai Huang, Shih-Yuan Chen, A compact slot loop rectenna for dual-band operation at 2.4-and 5.8-GHz bands, in: 2016 IEEE International Symposium on Antennas and Propagation (APSURSI), IEEE, 2016.
[21] Ha Vu Ngoc Anh, et al., Design of a dual-band rectenna for small IoT terminal, in: 2019 International Symposium on Electrical and Electronics Engineering (ISEE), IEEE, 2019.
[22] Minh Q. Dinh, Thuy Le Minh, Triplexer-based multiband rectenna for RF energy harvesting from 3G/4G and Wi-Fi, IEEE Microw. Wireless Compon. Lett. (31.9 2021) 1094–1097.
[23] Hamza Tafekirt, et al., A sensitive triple-band rectifier for energy harvesting applications, IEEE Access 8 (2020) 73659–73664.
[24] Mohamed Aboualalaa, Mansour Islam, K. Pokharel Ramesh, Energy harvesting rectenna using high-gain triple-band antenna for powering internet-of-things (IoT) devices in a smart office, IEEE Trans. Instrum. Meas. 1–12 (72) (2023).
[25] Zhen Li, et al., Two-port five-band rectenna for ultra-low ambient RF energy harvesting, IEEE Antenn. Wireless Propag. Lett. 22 (8) (2023) 419–426.
[26] Yuchao Wang, et al., Efficiency enhanced seven-band omnidirectional rectenna for RF energy harvesting, IEEE Trans. Antenn. Propag. (70.9) (2022) 8473–8484.
[27] Ping Lu, Chaoyun Song, Ka Ma Huang, Ultra-wideband rectenna using complementary resonant structure for microwave power transmission and energy harvesting, IEEE Trans. Microw. Theor. Tech. (69.7) (2021) 3452–3462.
[28] Devisowjanya Potti, et al., An ultra-wideband rectenna using optically transparent Vivaldi antenna for radio frequency energy harvesting, Int. J. RF Microw. Computer-Aided Eng. 30 (10) (2020) e22362.
[29] Euclides Lourenço Chuma, Yuzo Iano, Leonardo Lorenzo Bravo Roger, Ultra-wide band rectenna design with discone antenna and rectifier with high impedance inductor, in: 2021 5th International Symposium on Instrumentation Systems, Circuits and Transducers (INSCIT), IEEE, 2021.
[30] Lalbabu Prashad, Harish Chandra Mohanta, Heba G. Mohamed, A compact circular rectenna for RF-energy harvesting at ISM band, Micromachines 14 (4) (2023) 825.
[31] Shailendra Singh Ojha, Vandana Vikas Thakare, P.K. Singhal, Ultra-wideband rectenna with the dual ground plane for wide dynamic input power and load range, Int. J. Electron. 1–25 (2024).